HHS Public Access

Author manuscript

NMR Biomed. Author manuscript; available in PMC 2016 December 01.

Published in final edited form as:

NMR Biomed. 2015 December ; 28(12): 1707–1715. doi:10.1002/nbm.3430.

Spectral fitting using basis set modified by measured B_0 field distribution

Ningzhi Li, PhD, **Li An, PhD**, and **Jun Shen, PhD**

Molecular Imaging Branch, National Institute of Mental Health, National Institutes of Health, Bethesda, MD, USA

Abstract

This study sought to demonstrate and evaluate a novel spectral fitting method to improve quantification accuracy in the presence of large magnetic field distortion, especially with high fields. Magnetic resonance spectroscopy (MRS) experiments were performed using a point resolved spectroscopy (PRESS)-type sequence at 7 Tesla. A double-echo gradient echo (GRE) sequence was used to acquire B_0 maps following MRS experiments. The basis set was modified based on the measured B_0 distribution within the MRS voxel. Quantification results were obtained after fitting the measured MRS data using the modified basis set. The proposed method was validated using numerical Monte Carlo simulations, phantom measurements, and by comparing occipital lobe MRS measurements under homogeneous and inhomogeneous magnetic field conditions. *In vivo* results acquired from voxels placed at thalamus and prefrontal cortex regions close to the frontal sinus agreed well with published values. Instead of noise-amplifying complex division, the proposed method treats field variations as part of the signal model, thereby avoiding inherent statistical bias associated with regularization. Simulations and experiments showed that the proposed approach reliably quantified results in the presence of relatively large magnetic field distortion.

Keywords

Metabolite quantification; non-linear fitting; field map; prefrontal lobe; deep brain gray matter

INTRODUCTION

Brain neurochemistry has frequently been studied using *in vivo* magnetic resonance spectroscopy (MRS). Such studies have identified abnormal neurometabolite levels in various brain regions that provide insights into a range of brain disorders, including anxiety and affective disorders (1-4), obsessive-compulsive disorder (5,6), schizophrenia (4,7,8), and autism (9). Many of these studies reported neurometabolite differences between patients and healthy controls in cortical and deep brain regions. For example, abnormally low levels of N-Acetylaspartic acid (NAA) were found in the dorsolateral prefrontal cortex of

Correspondence Ningzhi Li, PhD, 10 Center Dr, 3D46, Bethesda, MD, USA, 21046, Telephone: 301-594-0962, Fax: 301-480-5904, ningzhi.li@nih.gov.

DISCLOSURES

The authors have no conflict of interest to disclose, financial or otherwise.

individuals with bipolar and unipolar mood disorders (1,2). Patients with social anxiety disorder showed changes in NAA and choline (Cho) levels in thalamus, caudate, and putamen of the basal ganglia circuitry (3). In addition, several studies reported that, compared to healthy controls, patients with obsessive-compulsive disorder had a higher NAA/creatine (Cr) ratio in the prefrontal cortex and left hippocampus and a lower ratio in the bilateral thalamus (5,6). Glutamate and glutamine (Glu+Gln) levels in the thalamus have also been found to correlate positively with schizophrenia symptoms (7,8). Furthermose, significantly decreased NAA concentrations have been reported in the bilateral orbitofrontal cortex of autistic patients (9).

Despite these interesting findings, it should be noted that the quality of MRS data can be severely affected by static magnetic field distortion in cortical regions close to the sinuses and in deep brain regions. Difficulties in acquiring high quality MRS data in brain regions with large magnetic field inhomogeneity have undoubtedly contributed to some of the controversies extant in the literature (4). Quantification in MRS is generally based on idealized model lineshape functions. However, the accuracy of spectral fitting using idealized model function is limited when there is severe lineshape distortion due to large static B_0 field inhomogeneities. Large susceptibility effects are present in the prefrontal cortex region where the frontal sinus is located. Deep brain structures such as the thalamus and basal ganglia are also associated with large susceptibility effects, partly due to iron deposition. B_0 field inhomogeneities due to large susceptibility effects are usually difficult to compensate for studies performed on most clinical scanners. For high magnetic field studies, uncompensated magnetic field distortion can largely offset any gains in spectral resolution associated with increased magnetic field strength. In the presence of large B_0 field inhomogeneities, spectral lineshape is significantly distorted and cannot be properly characterized by idealized lineshape model functions. Thus, using idealized lineshape models to fit the observed data may lead to unreliable metabolite concentrations.

One possible solution to this problem is changing the model function from a single Lorentzian or Gaussian type to a finite sum of Lorentzian and Gaussian type lines with the cost of increased fitting parameters (10). Another widely used method corrects lineshape distortions by complex division using a reference signal, such as the unsuppressed water signal (11). Because water signal usually decays faster than metabolite signal—especially at high magnetic fields—Tikhonov regularization (12) and Wiener filtering (13) have been introduced to lineshape deconvolution to mitigate noise amplification associated with complex division. Another deconvolution method uses the B_0 field map from a separate acquisition as the reference signal (14), and lineshape distortions derived from B_0 field inhomogeneities are removed via complex division using the free induction decay (FID) synthesized from B_0 distribution within the MRS voxel.

The current study presents a new approach for analyzing MRS data acquired from regions with large uncompensated magnetic field distortion. We used a separately acquired B_0 map to synthesize lineshape functions. Instead of complex division—which is prone to spike artifacts and noise amplification, and introduces statistical bias through regularization—we modified the spectral basis set based on the acquired B_0 map. The modified basis set was

then used to fit the *in vivo* MRS data. Since complex division was not used, this method did not require regularization.

THEORY

If an *in vivo* MRS voxel yields N different lines in the nuclear magnetic resonance (NMR) spectrum with offset frequencies ν_j and transverse relaxation time T_{2j} (1<j< J), the measured spectra $S(\nu)$ can be expressed by:

$$S(v) = f(v) * \sum_{j=1}^{J} A_j / \left[\frac{1}{T2_j} + i2\pi (v - v_j) \right] \quad [1a]$$

$$f(v) = \mathscr{F} \left(\int e^{-i\Delta\omega(\boldsymbol{r})t} d^3\boldsymbol{r} \right) \quad [1b]$$

where ν refers to frequencies; A_j is the individual peak amplitude; the integral $\int e^{i\Delta\omega(\boldsymbol{r})t}\, d^3\boldsymbol{r}$ is the FID synthesized from B_0 distributions ($\Delta\omega$) within the MRS voxel, where $\boldsymbol{r}$ indicates locations. $f(\nu)$ is the Fourier transform ($\mathscr{F}$) of the integral, acting as a convolution factor to the measured spectra. If the MRS voxel measures M_x, M_y, and M_z in three dimensions and the corresponding image voxel measures I_x, I_y, and I_z, the required number of pixels from the B_0 map for integration is:

$$N = \frac{M_x}{I_x} \cdot \frac{M_y}{I_y} \cdot \frac{M_z}{I_z} \quad [2]$$

Eq. 1b can be re-written as:

$$f(v) = \mathscr{F} \left(\sum_{n=1}^{N} e^{-i\Delta\omega_n t} \right) \quad [3]$$

Because B_0 distributions are relatively slow-varying within a spectroscopy voxel, image interpolation can be used as an alternative to time-consuming high resolution B_0 acquisitions.

The local field distribution can be computed based on phase difference and the time difference from a two-echo sequence. The distortion-free FID $S_c(t)$ could be obtained through deconvolution in the frequency domain, which equals complex division in the time domain:

$$S_c(t) = S(t) / \sum_{n=1}^{N} e^{-i\Delta\omega_n t} \quad [4]$$

However, because the FID synthesized from B_0 distribution usually decays more slowly than the metabolite FID, complex division only restores the part of metabolite FID that is above the noise level. This partial restoration leads to spike artifacts in the frequency domain. To avoid noise amplification due to complex division, regularization of Eq. 4 is usually necessary.

The spectral model function $S_m(\nu)$ linearly combines individual basis spectra simulated from density matrix with additional parameters that characterize quantification measures of concentrations, spectral linewidth, and spectral frequency shift. With a known field distribution function $f(\nu)$, a modified signal model $S_d(\nu)$ can be constructed:

$$S_d(v) = S_m(v) * f(v) \quad [5]$$

The aforementioned quantification parameters could be solved by minimizing the difference between the measured signal and the modified model signal in the least-square sense without bias-producing regularization:

$$min \| S(v) - S_d(v) \|^2 \quad [6]$$

MATERIALS AND METHODS

Monte Carlo Simulations

Monte Carlo simulations were performed to validate the proposed method and compare it with the frequently used lineshape deconvolution method based on unsuppressed water. The ideal FIDs were computed by multiplying trial concentration values and T_2 decay functions to the density matrix-simulated FIDs. Metabolites of NAA, N-acetyl-aspartyl-glutamate (NAAG), Glu, Gln, Cr, and Cho were simulated with trial concentrations of 13, 2.6, 10, 1.5, 10, and 3; and T_2 values of 130ms, 130ms, 90ms, 90ms, 90ms, and 150ms, respectively (15). The FID synthesized from the B_0 map was generated by integrating all pixels from the B_0 map within the MRS voxel from a typical *in vivo* study (*vide infra*). The *in vivo* MRS voxel was selected to cover the thalamus region where large susceptibility effects were present. The simulated metabolite FIDs were generated by multiplying the combined ideal FIDs by the synthesized FID from B_0 map plus random noise. The unsuppressed water FID was similarly generated, with a T_2 value of 45ms (15).

Two methods were used to fit the simulated metabolite FIDs. The proposed method generates a modified basis spectral model by applying the FID synthesized from the B_0 map to the basis set. Quantification results from the simulated metabolite FID were determined by minimizing the difference between reconstructed spectra from simulated FIDs and the modified signal model using non-linear fitting software developed in-house (13). Metabolite concentrations were also determined using the lineshape deconvolution method based on unsuppressed water FID with a regularization parameter of 0.007. The regularization parameter was determined using the L-curve method (12). Both methods were repeated 100 times with the same noise level but different realizations of random noise. Results from two methods were compared with the assigned trial concentrations. Simulations and fitting procedures were all programmed in Matlab (R2014a).

Phantom Studies

MRS data from spherical oil and water phantoms were collected on a Siemens 7T scanner equipped with a 32-channel receiver head coil using a point resolved spectroscopy (PRESS)-type sequence with radio frequency (RF) suppression and echo time (TE) optimization (16).

The water phantom contains metabolites including NAA, Cr, Cho, Glu, and myo-inositol (mI). The PRESS-type sequence was designed to spectrally resolve Glu and Gln. Acquisition parameters were: repetition time (TR): 2.5s; TE_1/TE_2: 69/37ms; voxel size: 2 or 3 cm isotropic, suppression pulse flip angle: 90°, spectral width: 4000Hz, number of data points: 2048, and number of transients: 128 with eight interleaved unsuppressed water acquisitions. In order to mimic an inhomogeneous magnetic field, shim currents were deliberately misadjusted. Immediately following the MRS acquisition, field map data were acquired using a double echo GRE sequence with the following acquisition parameters: TR: 657ms; TE_1/TE_2: 5.5/10.5ms; in-plane resolution: 3mm; slice thickness: 3mm. Or, TR: 700ms; TE_1/TE_2: 4.5/9.5ms; in-plane resolution: 1mm.

Phase maps (ϕ) were first unwrapped through a magnitude image-guided unwrapping algorithm (17). The B_0 distribution was then determined by the phase difference and time difference from two echoes:

$$\Delta\omega\left(x,y,z\right)=\frac{\varphi_1\left(x,y,z\right)-\varphi_2\left(x,y,z\right)}{\left(TE_1-TE_2\right)} \quad [7]$$

The offline processing pipeline can be divided into three steps. The first step prepared a single metabolite FID and a single water FID from the multi-coil and multi-transient measurements. In this step, metabolite FIDs from 128 acquisitions were first aligned after frequency and phase correction, and then averaged over different transients for each of 32 channels. The 32-channel FIDs were averaged using a generalized least square method to yield a single metabolite FID (18). The single water FID was similarly computed and was subsequently used to remove eddy current effects. In the second step, the modified spectra signal model was constructed following Eq. 5 by applying the FID synthesized from the B_0 map to the basis set signal model. In the final step, fitting software developed in-house and programmed in Matlab (R2014a) solved metabolite concentrations by minimizing the difference between reconstructed spectra from measured data and the modified signal model in a least-square sense. Besides regular quantification parameters, the minimization procedure also included a cubic spline baseline function with eight control parameters compensating for baseline distortion (16). The same post-processing pipeline was applied to each MRS dataset. Quantification results from the homogeneous field acquisition were used as the ground truth reference. Metabolite concentrations from inhomogeneous fields were then compared with the ground truth references.

In Vivo Studies

Twelve healthy volunteers (two male, 10 female, ages 22 to 38) were scanned on a Siemens 7T scanner equipped with a 32-channel receiver head coil. All procedures were approved by the institutional review board (IRB) of the NIMH. Written informed consent was obtained from all participants.

Seven healthy volunteers were scanned in the occipital lobe to validate the proposed method. Before the MRS study, a high-resolution 3D T1-weighted MP-RAGE (magnetization prepared rapid gradient echo) sequence was used to locate the MRS voxel in

a white matter-dominated area of the occipital lobe for each subject. Acquisition parameters were: TR: 3s; TE: 3.9ms; voxel size: 1mm isotropic. Two sets of MRS data were acquired from the same voxel of each subject using the PRESS-type sequence (16). First and second order B_0 shim coefficients were adjusted using FASTMAP (19) to achieve an essentially homogeneous magnetic field within the MRS voxel for the first dataset. The second dataset was acquired after manually misadjusting the first order shimming coefficients by approximately 20%. The first dataset with homogeneous field was treated as the approximate ground truth reference. Acquisition parameters for the PRESS-type sequence were: TR: 2.5s; TE_1/TE_2: 26/72ms; voxel size: 2cm isotropic. Immediately following each MRS data acquisition, the field map dataset was sampled using a double-echo GRE sequence with imaging parameters: TR: 700ms; TE_1/TE_2: 4.5/9.5ms; in-plane resolution: 1mm; slice thickness: 3mm. The data processing pipeline was the same as the phantom studies. Because Cr is a relatively stable metabolite, quantification precision of the new method was evaluated by comparing metabolite over Cr concentrations from the inhomogeneous field acquisition with the ground truth reference.

Five *in vivo* MRS datasets were also acquired from the thalamic region and from prefrontal cortex regions. The prefrontal cortex voxel was placed close to the frontal sinus. Due to large susceptibility effects, relatively large B_0 field inhomogeneities were present in both regions after shimming. All sequence parameters and data processing pipelines were the same as in the occipital lobe experiments described above.

RESULTS

Monte Carlo Simulation

Figure 1 displays Monte Carlo simulation results of reconstructed spectra processed using the proposed method (left panel) as well as the regularized lineshape deconvolution method based on unsuppressed water signal (right panel). In each subfigure, the top trace was reconstructed from an FID with field distortion from an *in vivo* study and added Gaussian noise. The second trace from the top was reconstructed using parameters obtained from the spectral fitting procedure. The bottom two traces are baseline and residuals between the simulated spectrum and the reconstructed spectrum. Spike artifacts in the right subfigure are due to lineshape deconvolution where the decay rate of the reference signal was substantially different from the metabolite signals. In this case, the reference water signal decayed much faster than the metabolite signal. Comparison of quantification results from 100 simulations with known ground truth concentrations and different noise realizations are displayed in Figure 2. The proposed method, which was free of spike artifacts and statistical bias associated with regularization, yielded greatly improved accuracy compared with the lineshape deconvolution method. Because the water signal decayed much faster than the metabolite signal due to large B_0 field inhomogeneities at 7 Tesla, as expected, the regularized-unsuppressed water method had relatively large quantification errors.

Phantom study

Figure 3 shows typical spike artifacts in conventional lineshape deconvolution when metabolite signals decay faster than the reference signal. FID synthesized from the B_0 map

was used as the lineshape reference. As shown in the left panel of Figure 3, in the presence of severe B_0 inhomogeneity, dividing an FID signal synthesized from the B_0 map into the metabolite FID (black) only restored the part of the metabolite FID signal above the noise level (blue). This partial restoration led to spike artifacts in the frequency domain after Fourier transformation (arrows in right panel).

To evaluate the robustness of the proposed method, we manually distorted the magnetic field in the second phantom study. Reconstructed spectra from the second phantom study with different B_0 field inhomogeneities are shown in Figure 4. The top traces were reconstructed from measured spectral data. In the left subfigure, the magnetic field was shimmed by FASTMAP. In the middle and right subfigures, the field was distorted by misadjusting the first order shim currents by 20% and 40%, respectively. The second traces from the top were linearly combined by fitting results based on basis set spectra modified by the measured B_0 maps. The bottom two traces are baseline and residuals between the top two traces. Quantification results are shown as bar graphs in Figure 5. Compared to the ground truth reference, metabolite concentrations, as expected, tended to deviate further as the background field inhomogeneity became progressively larger. In Figure 4 and 5, the linewidth of the NAA signal was increased approximately four- and eight-fold under the first and second inhomogeneity conditions, respectively.

In Vivo studies

Figure 6 displays typical occipital lobe results from the *in vivo* method validation studies using healthy volunteers. MRS voxel locations are indicated by the yellow box overlaid on the axial and sagittal high resolution T_1-weighted images. For each subfigure, from top to bottom are reconstructed spectrum from measured FID, fitted spectrum, baseline and residuals between reconstructed spectrum and fitted spectrum. Despite deliberate misadjustment of shim currents for spectra on the right column of Figure 6, all spectra from the seven subjects yielded small residuals. Quantification results for major metabolites are displayed as bar graphs in Figure 7. Compared to the ground truth references estimated under homogeneous field conditions, most quantification results from inhomogeneous field acquisition yielded less than 5% error. The mean quantification errors across seven subjects are 0.9% for NAA, 1.18% for Cho, 0.74% for Glu and −2.10% for Gln.

Results from thalamic and prefrontal cortical voxels are displayed in Figures 8 and 9, respectively. For each subfigure, from top to bottom are reconstructed spectrum from measured FID, fitted spectrum, baseline and residuals between reconstructed spectrum and fitted spectrum. Quantification results for the thalamus and prefrontal cortex studies are summarized in Tables 1 and 2. Previous published metabolite values were calculated as metabolite to Cr concentration ratios and compared with our quantification results. Our quantification results were generally within the range of previously published values (1-3, 7-9, 20, 21).

DISCUSSION

Metabolite quantification in cortical and deep brain gray matters may provide important biomarkers for a variety of neurological and psychiatric disorders. However, large

susceptibility effects in basal ganglia, hippocampal, thalamic, and prefrontal cortex areas cause large spectral lineshape distortions, and introduce significant errors when fitting the distorted spectra using idealized lineshape models. Lineshape distortions may be corrected by complex division using a reference signal such as the unsuppressed water signal, or a synthesized signal using the acquired B_0 distribution. In this type of methods, regularization (either in the form of Tikhonov regularization or Wiener filtering) is required to avoid disastrous noise amplification at zero crossings (12, 13). In both Tikhonov regularization and Wiener filtering, the linear square solution is modified. As a result, these methods introduce inherent systematic errors (i.e., statistical bias) to metabolite quantification (22). In addition, because the reference signal often decays at a different rate from the metabolite signals, spike artifacts are generated; these must be carefully avoided so as not to confound MRS measurements. The widely used MRS data processing software LCModel (23) uses a built-in regularized and constrained model-free lineshape function to account for lineshape distortions. Because all regularization procedures skew the unbiased least square solution, lineshape regularization in LCModel generates statistical bias (24). At the cost of extra scans, the proposed method experimentally determines the lineshape function by measuring the B_0 map. Removing lineshape function from parameters to be determined by fitting can minimize the possibility of an inaccurate lineshape function and reduces the degree of freedom in fitting. Since no regularization is involved, the proposed method leads to the unbiased solution.

The present study used a modified signal model to minimize the difference between the observed signal and the signal model as an alternative to existing approaches. In particular, the signal model was modified by the same amount of lineshape distortion introduced by the B_0 field inhomogeneities. This was achieved by measuring the magnetic field using standard B_0 mapping and applying the measured B_0 distribution to the idealized lineshape model. The modified lineshape model was then employed to fit the measured metabolite data. One key advantage of this method is that complex multiplication instead of complex division was needed to achieve effective lineshape deconvolution. As such, the method avoids the noise amplification associated with complex division and no bias-producing regularization is required. This novel approach significantly improved the accuracy and reliability of spectral fitting in the presence of large magnetic field distortion. Since complex division has been used in a variety of lineshape correction schemes in MRS and NMR in general, we expect that the general idea proposed here will find other applications (e.g., in eddy current correction by reference signals).

Accurate and rapid measurement of the field map is a key step in this method. A variety of B_0 mapping methods have been proposed in the literature. The gold standard and most accurate B_0 mapping method collects multiple closely spaced phase data, and calculates the phase slope verse echo time from a linear square error fit. Another widely used method computes the B_0 map by measuring the linear phase shift in the frequency domain. Rapid B_0 mapping can also be achieved by using echo planar readout gradient train (25) or modified k-space trajectory (in which the center of the k-space is sampled twice (26)). Although we used a simple gradient echo method, multi-echo data point fitting may further improve the accuracy of metabolite quantification, while the echo planar readout could accelerate field map data sampling.

The single voxel MRS samples data from a small region of the human brain. On the other hand, the B_0 map acquired using the standard double echo-GRE sequence covers the whole brain slices. The current study calculated a synthesized signal from image pixels that matches the locations inside the MRS voxel. As the B_0 map covers more brain regions, the synthesized signal could be calculated from any locations within it. The current method can be easily extended to multi-voxel MRS or magnetic resonance spectroscopic imaging (MRSI). For both multi-voxel MRS and MRSI, while spectra are acquired from different brain locations to measure the metabolite variations, the B_0 field map only requires a single acquisition.

The Monte Carlo simulation study numerically validated our proposed method. Phantom studies validate the accuracy of lineshpae generated from B_0 maps using non-overlapping signals from NAA, Glu, Cr, Cho and mI under different field inhomogeneous conditions. The benefit of using non-overlapping signal is to separate the effects of lineshape function from those of overlapping signals. Since the *in vivo* ground truth values of metabolites were unknown, we used a voxel placed in the occipital lobe and compared metabolite quantification results under homogeneous and inhomogeneous B_0 distributions. The occipital lobe is far from the sinus. The occipital voxel is also close to the isocenter of the magnetic field. Thus, the MRS voxel located in the occipital lobe can be shimmed very well. In this study, the mean NAA linewidth under the first field homogeneity condition was 10.27+1.33Hz, indicating excellent B_0 homogeneity after adjusting both first- and second-order shim currents. We were able to use the well-shimmed occipital lobe spectra as the approximate ground truth reference to validate the proposed data fitting method based on complex multiplication. It is worthwhile to mention that although FASTMAP technique (19) has been used in this study, the more optimal shimming technique FASTEST MAP (25) could further improve field homogeneities and thus offers more reliable reference values. As shown in Figure 5, the mean quantification errors across the seven subjects under inhomogeneous B_0 distribution in the occipital lobe voxel were fairly small, providing strong *in vivo* validation of the proposed method. In particular and as expected, no significant systematic error was observed in metabolite quantification due to our complex-multiplication-based lineshape correction procedure as evidenced by the fact that errors with respect to the approximate ground truth values were markedly reduced upon averaging across the seven subjects.

All voxels in the current study were carefully chosen to avoid significant cerebrospinal fluid (CSF) space. However, the composition of the MRS voxel should be considered when significant amount of CSF enters the spectroscopic volume. In particular, the B_0 pixels corresponding to the CSF should be taken out of the lineshape function synthesized from B_0 map (the integral in Eq. 3). Because T_2 of CSF (~1500ms) is much longer than T_2 of brain tissue (~80ms-110ms), intensity based-segmentation could be easily applied to remove pixels originated from CSF.

Tables 1 and 2 show relatively large range in reported metabolite concentrations in the thalamus and prefrontal cortical regions. In addition to variations attributable to differences in anatomy, age, sex, and MRS method, the difficulties in acquiring high quality MRS data and fitting them also contributed to the reported discrepancies. Furthermore, previous

publications are all based on relatively small sample sizes and relatively low magnetic field strength. With the above qualifications, our thalamus and prefrontal cortical results generally agree with values previously reported in the literature. However, we would expect this proposed method to fail when B_0 field inhomogeneities are very severe, and used phantom studies to evaluate the limitations of our novel method. When NAA linewidth was increased by approximately eight times in the second inhomogeneity condition, the error was still within 6.5% (see Figure 4 and 5). Therefore, we do not expect large errors in our thalamus and prefrontal cortex results although the ground truth values were unknown in this case. The unknown ground truth values in these two locations remain a limitation of our study.

Unlike spectral editing methods that directly resolve signal of interest and can be used to quantify metabolites with low concentrations, the current method only treats lineshape distortion caused by B_0 field inhomogeneity. As such, it is limited for quantifying metabolites that are known to have spectral interference and exist at low concentration.

Many clinical questions require the assessment of brain regions with large susceptibility effects. For example, most psychiatric diseases involve the frontal lobe. A general increase in the quality of MRS data acquired from regions close to the frontal sinus will thus be of great value to the field of psychiatric MRS. In addition, the problem of lineshape distortion is expected to be further aggravated by the continued growth of high magnetic field applications. Figure 1 and 2 show that at 7 Tesla, the new method markedly outperformed the Tikhonov regularization-based lineshape deconvolution method. This is not surprising considering the much shorter tissue water decay at 7 Tesla, which makes it harder to use any tissue water-based lineshape deconvolution schemes. Therefore, we expect that the proposed method will be generally useful for enhancing the quality of clinical MRS data acquired from brain regions associated with relatively large magnetic field distortions after shimming.

In conclusion, the present study demonstrates and evaluates a novel approach to spectral fitting that can be used in the presence of large magnetic field distortion, especially at high fields. The magnetic field distribution was first measured through standard B_0 mapping. An FID synthesized from the magnetic field distribution within the MRS voxel was then applied to the basis set. The modified basis set was used to fit *in vivo* MRS data. Monte Carlo simulations showed that the proposed approach yielded fewer errors compared to the frequently used unsuppressed water method. Phantom and *in vivo* validation experiments showed that the proposed approach provides reliable and improved quantification results in the presence of relatively large magnetic field distortion.

Supplementary Material

Refer to Web version on PubMed Central for supplementary material.

ACKNOWLEDGMENTS

The authors thank Mr. Christopher Johnson and Dr. Steve Li for recruiting and consenting healthy volunteers, and Ms. Ioline Henter for excellent editorial assistance.

This work was supported by the Intramural Research Program of the National Institute of Mental Health, National Institutes of Health (IRP-NIMH-NIH; Protocol:11-M-0045).

Abbreviations

Cho	choline
Cr	creatine
FID	free induction decay
Gln	glutamine
Glu	glutamate
GRE	gradient echo
mI	myo-inositol
MRS	magnetic resonance spectroscopy
NAA	N-Acetylaspartic acid
NAAG	N-acetyl-aspartyl-glutamate
NMR	nuclear magnetic resonance
ϕ	phase maps
PRESS	Point resolved spectroscopy
RF	radio frequency
TE	time echo
TR	repetition time
MRSI	magnetic resonance spectroscopic imaging

REFERENCES

1. Brambilla P, Stanley JA, Nicoletti MA, Sassi RB, Mallinger AG, Frank E, Kupfer D, Keshavan MS, Soares JC. ^{1}H magnetic resonance spectroscopy investigation of the dorsolateral prefrontal cortex in bipolar disorder patients. J Affect Disord. 2005; 86:61–67. [PubMed: 15820271]
2. Brambilla P, Stanley JA, Nicoletti MA, Sassi RB, Mallinger AG, Frank E, Kupfer D, Keshavan MS, Soares JC. ^{1}H magnetic resonance spectroscopy study of the dorsolateral prefrontal cortex in unipolar mood disorder patients. Psychiatry Res. 2005; 138:131–139. [PubMed: 15766636]
3. Howells FM, Hattingh CJ, Syal S, Breet E, Stein DJ, Lochner C. ^{1}H-magnetic resonance spectroscopy in social anxiety disorder. Prog Neuropsychopharmacol Biol Psychiatry. 2015; 58:97–104. [PubMed: 25549832]
4. Kraguljac NV, Reid MA, White D, Jones R, den Hollander J, Lowman D, Lahti AC. Neurometabolites in schizophrenia and bipolar disorder — a systematic review and meta-analysis. Psychiatry Res. 2012; 203:111–125. [PubMed: 22981426]
5. Lu YR, Lin Z, Li HC. ^{1}H magnetic resonance spectroscopy imaging of prefrontal region and hippocampus in patients with obsessive-compulsive disorder. Zhejiang Med J. 2007; 29:226–228.
6. Fan Q, Tan L, You C, Wang J, Ross CA, Wang X, Zhang T, Li J, Chen K, Xiao Z. Increased N-acetylaspartate/creatine ratio in the medical prefrontal cortex among unmedicated obsessive-compulsive disorder patients. Psychiatry Clin Neurosci. 2010; 64:483–490. [PubMed: 20923427]
7. Hugdahl, Kenneth; Craven, AR.; Nygard, M.; Loberg, EM.; Berle, JO.; Johnsen, E.; Kroken, R.; Specht, K.; Andreassen, OA.; Ersland, L. Glutamate as a medicating transmitter for auditory hallucinations in schizophrenia: A ^{1}H MRS study. Schizophr Res. 2015; 161:252–60. [PubMed: 25542859]

8. Tandon N, Bolo NR, Sanghavi K, Mathew IT, Francis AN, Stanley JA, Keshavan MS. Brain metabolite alterations in young adults at familial high risk for schizophrenia using proton magnetic resonance spectroscopy. Schizophr Res. 2013; 148:59–66. [PubMed: 23791389]
9. Mori K, Toda Y, Ito H, Mori T, Goji A, Fujii E, Miyazaki M, Harada M, Kagami S. A proton magnetic resonance spectroscopic study in autism spectrum disorders: Amygdala and orbito-frontal cortex. Brain Dev. 2013; 35:139–45. [PubMed: 23114054]
10. Cavassila S, Deval S, Huegen C, van Ormondt D, Graveron-Demilly D. Cramer-Rao bounds: an evaluation tool for quantitation. NMR Biomed. 2001; 14:278–283. [PubMed: 11410946]
11. de Graaf AA, van Dijk JE, Bovee WM. QUALITY: quantification improvement by converting lineshapes to the Lorentzian type. Magn Reson Med. 1990; 13:343–357. [PubMed: 2325535]
12. Zhang Y, Li S, Marenco S, Shen J. Quantitative measurement of N-Acetyl-aspartyl-glutamate at 3T using TE-averaged PRESS spectroscopy and regularized lineshape deconvolution. Magn Reson Med. 2011; 66:307–313. [PubMed: 21656565]
13. An L, Li S, Wood ET, Reich DS, Shen J. N-acetyl-aspartyl-glutamate detection in the human brain at 7 Tesla by echo time optimization and improved Wiener filtering. Magn Reson Med. 2014; 72:903–912. [PubMed: 24243344]
14. Dong Z, Peterson BS. Spectral resolution amelioration by deconvolution (SPREAD) in MR spectroscopic imaging. J Magn Reson Imag. 2009; 29:1395–1405.
15. Marjanska M, Auerbach EJ, Valabregue R, Van de Moortele PF, Adriany G, Garwood M. Localized H-1 NMR spectroscopy in different regions of human brain *in vivo* at 7T: T-2 relaxation times and concentrations of cerebral metabolites. NMR Biomed. 2012; 25:332–339. [PubMed: 21796710]
16. An L, Li S, Murdoch JB, Araneta MF, Johnson C, Shen J. Detection of glutamate, glutamine, and glutathione by radiofrequency suppression and echo time optimization at 7 Tesla. Magn Reson Med. 2015; 73:451–458. [PubMed: 24585452]
17. Cusack R, Papadakis N. New robust 3-D phase unwrapping algorithms: application to magnetic field mapping and undistorting echo planar images. Neuroimage. 2002; 16:754–764. [PubMed: 12169259]
18. An L, van der Veen JW, Li S, Thomasson DM, Shen J. Combination of multichannel single-voxel MRS signals using generalized least squares. J Magn Reson Imag. 2013; 37:1445–1450.
19. Gruetter R. Automatic, localized in vivo adjustment of all first- and second-order shim coils. Magn Reson Med. 1993; 29:804–811. [PubMed: 8350724]
20. Geurts JJG, Barkhof F, Castelijns JA, Uitdehaag BMJ, Polman CH, Pouwels PJW. Quantitative ^{1}H-MRS of healthy human cortex, hippocampus, and thalamus: Metabolite concentrations, quantification precision, and reproducibility. J Magn Reson Imag. 2004; 20:366–371.
21. Choi C, Dimitrov IE, Douglas D, Patel A, Kaiser LG, Amezcua CA, Maher EA. Improvement of resolution for brain coupled metabolites by optimized ^{1}H MRS at 7T. NMR Biomed. 2010; 23:1044–1052. [PubMed: 20963800]
22. Strang, G. Optimization and minimum principles: Regularized least squares. Wellesley-Cambridge Press; Wellesley MA: 2007. Computational science and engineering; p. 613-626.
23. Provencher SW. Estimation of metabolite concentrations from localized in vivo proton NMR spectra. Magn Reson Med. 1993; 30:672–679. [PubMed: 8139448]
24. Provencher SW. A constrained regularization method for inverting data represented by linear algebraic or integral equations. Comput Phys Commun. 1982; 27:213–227.
25. Tkac I, Gruetter R. Field mapping without reference scan using asymmetric echo-planar techniques. Magn Reson Med. 2000; 43:319–323. [PubMed: 10680699]
26. Roopchansingh V, Cox RW, Jesmanowicz A, Ward BD, Hyde JS. Single-shot magnetic field mapping embedded in echo-planar time-course imaging. Magn Reson Med. 2003; 50:839–843. [PubMed: 14523971]

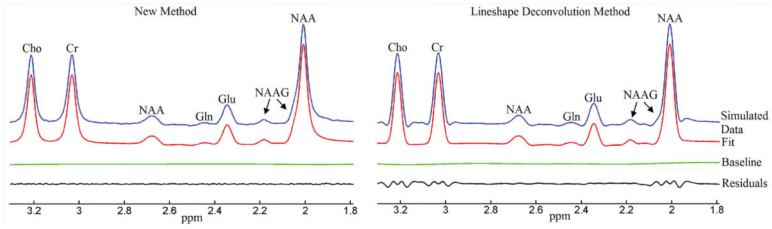

Figure 1.

Linear combination fitting plots by the proposed method (left) and the line-shape deconvolution method based on unsuppressed water signal (right). Spike artifacts in the right panel were due to lineshape deconvolution when the reference signal and the metabolite signals decayed at different rates.

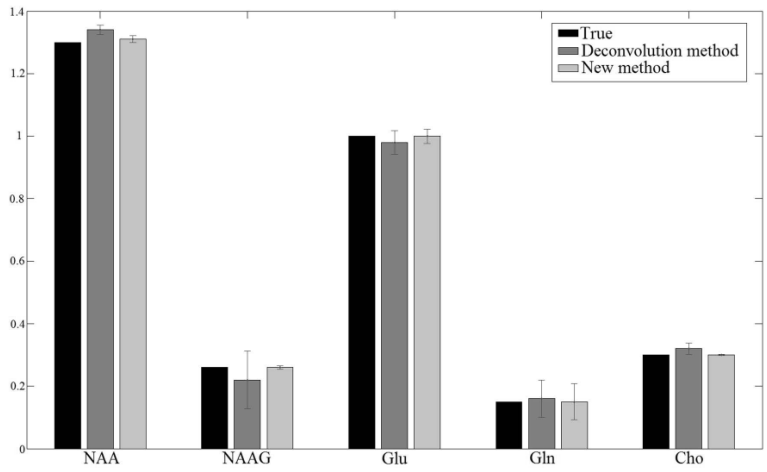

Figure 2.

Mean and standard deviation of metabolite/Cr concentration ratios from 100 simulations with different noise realizations. Black, dark gray and light gray bars represent ground truth concentrations, simulations from regularized unsuppressed water method and the proposed method, respectively. Maximum quantification error for the water method is 14.31% and for the proposed method is 2.67%. The exact concentration numbers are provided in Table 1 of supplemental information.

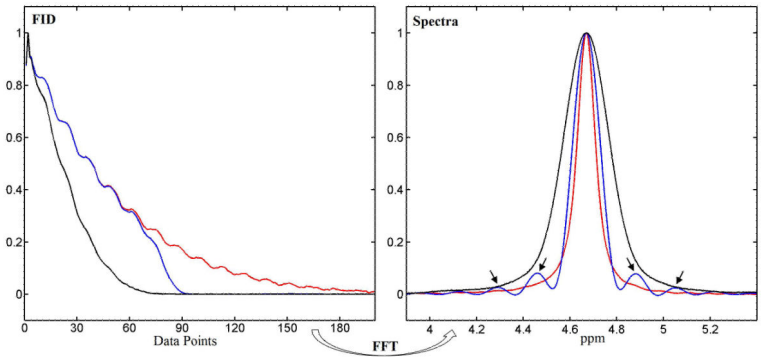

Figure 3.

Left panel: Oil phantom free induction decays (FIDs) acquired with homogeneous B_0 field (red) and inhomogeneous B_0 field (black). The latter was partially restored by complex division (blue). Right panel: corresponding spectra. Arrows indicate spike artifacts.

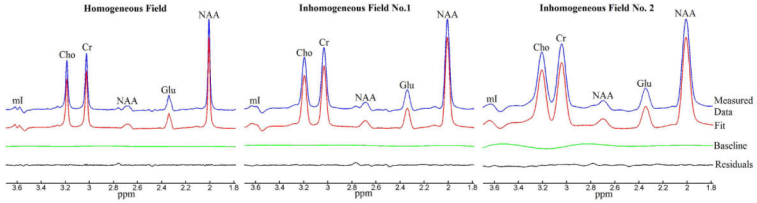

Figure 4.

Linear combination fitting plots of metabolite aqueous phantom data acquired at three different B_0 field inhomogeneities. Five metabolites were analyzed: NAA, Cho, Cr, Glu and mI. The small signal around 2.76 ppm was not included in the spectral model.

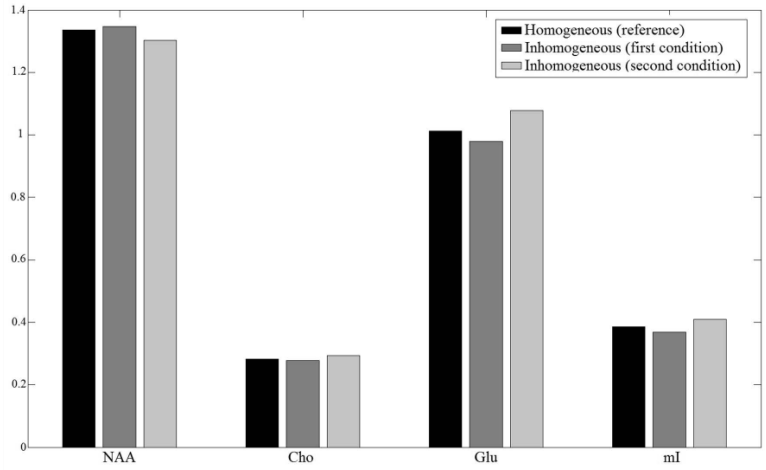

Figure 5.

Phantom metabolite/Cr concentration ratios from acquisitions with homogeneous field (black bar) and two different inhomogeneous fields (dark and light gray bars). The exact concentration numbers are provided in Table 2 of supplemental information.

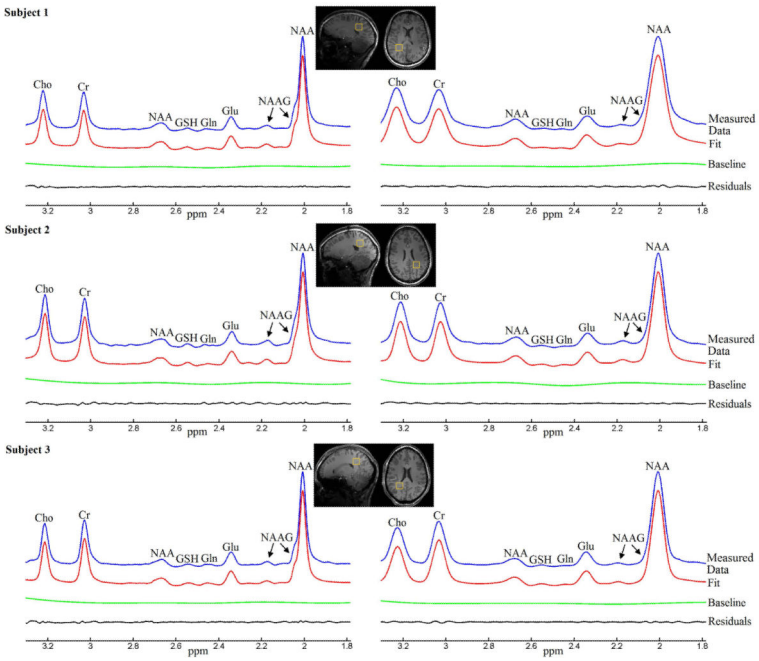

Figure 6.

Linear combination fitting plots from homogeneous field acquisition (left panels) and inhomogeneous field acquisition (right panels) of three healthy volunteers (different rows). The two acquisitions of each individual subject are from the same voxel located in the occipital lobe, indicated by the yellow boxes on the sagittal and axial T1-weighted images.

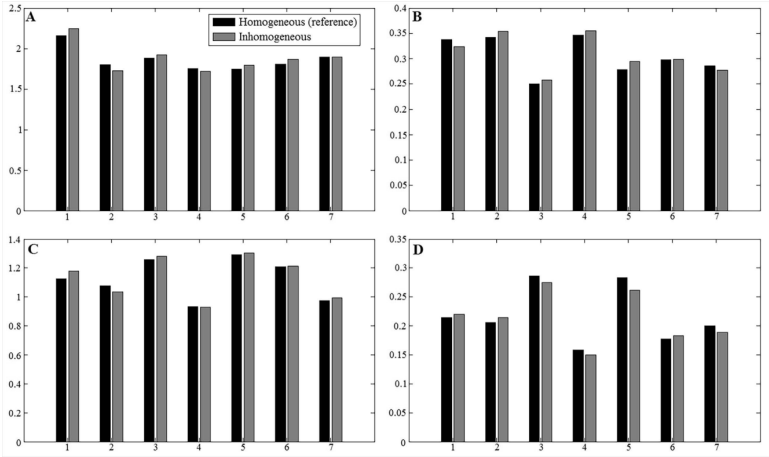

Figure 7.

Metabolite/Cr concentration ratios from homogeneous (black bar) and inhomogeneous field (gray bar) acquisitions of seven healthy volunteers. Four different chemicals are compared here, including NAA (A), Cho (B), Glu (C) and Gln (D). The mean quantification errors across seven subjects are 0.9% for NAA, 1.18% for Cho, 0.74% for Glu and −2.10% for Gln. The exact concentration numbers are provided in Table 3 of supplemental information.

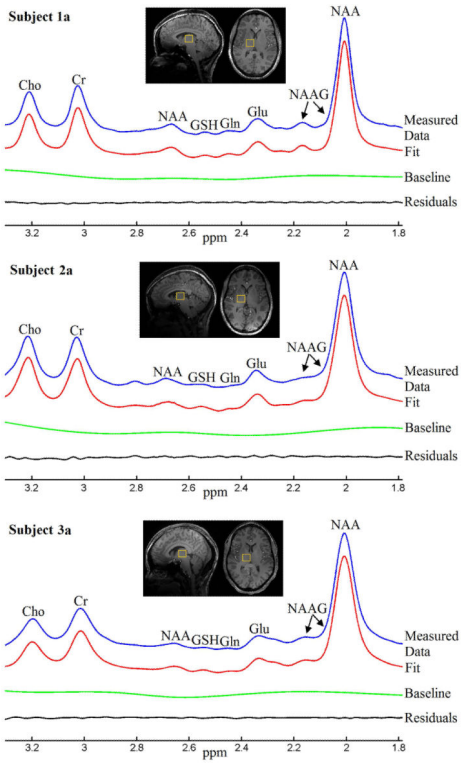

Figure 8.

Linear combination fitting plots from the thalamic regions of three healthy volunteers. The MRS voxels, indicated by the yellow boxes in the sagittal and axial T1-weighted images, cover the entire thalamus.

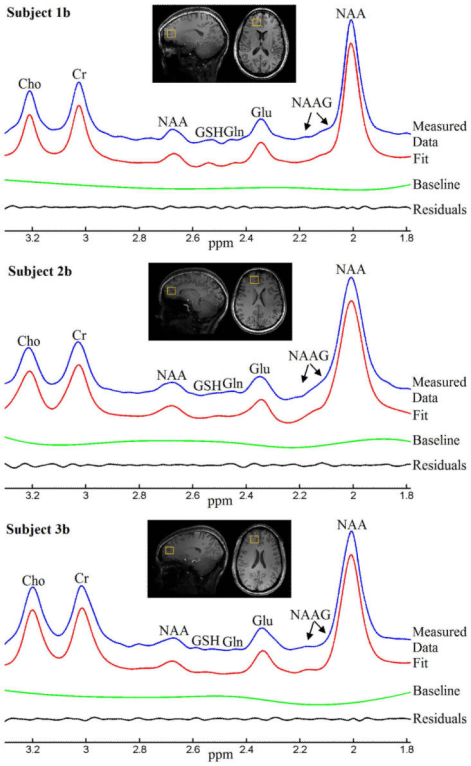

Figure 9.

Linear combination fitting plots from the prefrontal lobe voxel of three healthy volunteers. The MRS voxels were marked by the yellow boxes in the sagittal and axial T1-weighted images.

TABLE 1

Metabolite/Creatine concentration ratios from thalamic voxel

Chemicals	NAA	CHO	GLU	GLN
Subject1a	2.0543	0.4034	1.2623	0.2078
Subject2a	1.7423	0.2870	0.9685	0.1641
Subject3a	1.5167	0.4095	1.1483	0.1517
Subject4a	1.4809	0.2949	1.1449	0.2127
Subject5a	1.3499	0.3217	1.4406	0.2995
Mean±Std	**1.63±0.28**	**0.34±0.06**	**1.19±0.17**	**0.21±0.06**
Published *	**0.95-1.63**	**0.20-0.33**	**0.77-1.48**	**0.09-0.79**

* Published values were obtained from references 3, 8, and 20

Abbreviations: NAA: N-acetylaspartic acid; Cho: choline; Glu: glutamate; Gln: glutamine

TABLE 2

Metabolite/Creatine concentration ratios from prefrontal lobe voxel

Chemicals	NAA	CHO	GLU	GLN
Subject1b	2.1502	0.2636	1.1505	0.2765
Subject2b	1.4570	0.3126	1.1605	0.1008
Subject3b	1.6491	0.3089	1.6001	0.5335
Subject4b	1.7694	0.2770	1.3081	0.4813
Subject5b	1.4736	0.3242	1.1660	0.1683
Mean±Std	**1.70±0.28**	**0.30±0.03**	**1.28±0.19**	**0.31±0.19**
Published *	**1.03-2.00**	**0.12-0.75**	**1.05-1.27**	**0.26-0.36**

* Published values were obtained from references 1, 2, 7, 9, and 21

Abbreviations: NAA: N-acetylaspartic acid; Cho: choline; Glu: glutamate; Gln: glutamine